A Reliable Experimental Methodology for the Study of Wind-Turbine Rotor Blade Aerodynamics

IOP Conf. Series: Journal of Physics: Conf. Series **1222** (2019) 012001 doi:10.1088/1742-6596/1222/1/012001

A Reliable Experimental Methodology for the Study of Wind-Turbine Rotor Blade Aerodynamics

M Costantini[1], C Fuchs[1], U Henne[1], C Klein[1], V Ondrus[2], M Bruse[3], M Löhr[3], M Jacobs[3]

[1]DLR, Bunsenstrasse 10, D-37073 Göttingen, Germany
[2]University of Hohenheim, Garbenstrasse 30, D-70599 Stuttgart, Germany
[3]DNW, Bunsenstrasse 10, D-37073 Göttingen, Germany

E-mail: marco.costantini@dlr.de

Abstract. The aerodynamic performance of airfoils and blades designed for modern wind-turbine rotors, which have diameters of the order of hundred meters, must be examined at chord Reynolds numbers matching those of practical applications. In general, such high Reynolds numbers cannot be achieved in conventional wind tunnels. Moreover, knowledge on the boundary-layer transition location is essential to evaluate airfoil and blade performance at these flow conditions. This work presents an experimental methodology that can be applied at flow conditions reproducing those of real wind-turbine rotor blades and simultaneously provides aerodynamic coefficients and transition locations. The experimental methodology consists of: the Temperature-Sensitive Paint (TSP) technique for global, non-intrusive and reliable transition detection; conventional pressure measurements for the determination of the aerodynamic coefficients; and the High Pressure Wind Tunnel Göttingen (DNW-HDG) to run the experiments at Reynolds numbers matching those of real applications. The obtained results can be used to verify airfoil and blade performance and to validate numerical predictions. In the present work, the experimental methodology was applied to systematically investigate the aerodynamic performance of an airfoil designed for the mid-span sections of modern wind-turbine rotor blades. The examined chord Reynolds numbers were as high as 12 million and the angle-of-attack ranged from -14° to +20°. The presented methodology was here demonstrated to be mature for productive testing.

1. Introduction

Rotor blade aerodynamics has an essential role in overall wind-turbine performance and has continuously improved in the last decades. Airfoil classes have been specifically developed for wind-turbine rotor blades [1], with airfoil size and shape optimized for the different blade sections to satisfy aerodynamic and structural demands. Especially the airfoils for mid-span and outboard sections, however, are subjected to Reynolds number and roughness effects [1-3]; both these effects are related to the occurrence of boundary-layer transition on the airfoils under practical conditions. Transition occurring more upstream than design leads to significantly higher drag [4], lower lift and thus also to a lower lift-to-drag ratio [2,5]. It is therefore of fundamental importance to design airfoils for mid-span and outboard sections that present low sensitivity to roughness [1-2,5] and experimentally verify their performance at Reynolds numbers relevant for modern wind turbines with large rotor diameters (which can be of the order of 100 m).

In the mid-span area of modern wind-turbine rotor blades, the Reynolds number $Re = U_\infty c/\nu_\infty$ (where U_∞ and ν_∞ are the freestream velocity and kinematic viscosity, respectively, and c the airfoil chord length) can reach values of $10 \cdot 10^6$, or even higher [6]. Experiments in wind tunnels allow the systematic analysis of the aerodynamic performance of airfoils / blades and the validation of numerical predictions, but the maximal Reynolds number achievable in conventional wind tunnels is typically $6 \cdot 10^6$ [2]. While maintaining the freestream Mach number below M = 0.3, the Reynolds number can be further increased by increasing the gas kinematic viscosity. This can be accomplished in two ways: by decreasing the gas temperature, as in the case of cryogenic wind tunnels such as the Cryogenic Wind Tunnel Cologne (DNW-KKK) [6-8], or by increasing the gas pressure, as done in the High Pressure Wind Tunnel Göttingen (DNW-HDG) [9-12]. In this manner, the aerodynamic performance of airfoils developed for modern wind-turbine rotor blades can be studied in the appropriate Reynolds number range, thus avoiding that the experimental data are affected by the influence of a Reynolds number different from that achieved in practical applications.

Aerodynamic performance is typically examined in wind tunnels by measuring aerodynamic loads [1-2,5-6,8,11-12]. In general, these measurements do not provide any information (if any, only indirectly) on the airfoil / blade boundary-layer state and on the laminar-turbulent transition, which is however crucial for the evaluation and further improvement of the aerodynamic performance of rotor blades. This information can be provided by one or more rows of sensors, such as unsteady pressure sensors [8] or hot films [3], but they have intrinsically low spatial resolution; moreover, they can induce significant disturbances into the thin boundary layer developing on the wind-tunnel model surface at high Reynolds numbers. Global, non-intrusive and reliable transition measurements can be carried out by means of thermographic methods, such as Infra-Red (IR) thermography [3,13-14] and the Temperature-Sensitive Paint (TSP) technique [7,10,15-19]. IR thermography is widely used for transition detection at ambient conditions, but it cannot be applied easily at the low temperatures or at the high pressures needed to match the high Reynolds numbers of real wind-turbine rotor blades [10,15]. Transition measurements under these test conditions can be successfully conducted via TSP [6-7,10,16-19].

In the present study, the aerodynamic performance of an airfoil designed for the mid-span region of modern wind-turbine rotor blades was systematically investigated at high chord Reynolds numbers (up to $Re = 12 \cdot 10^6$) for a wide range of angles-of-attack (from -14° to 20°) in the DNW-HDG wind tunnel. The present work is built on and extends the investigations presented in [19]. Boundary-layer transition on the model upper surface was measured globally by means of TSP, while the coefficients of airfoil lift, drag and pitching moment were obtained via integration of the pressure distributions measured on the wind-tunnel model surface and in the model wake.

2. Experimental Setup

The investigated two-dimensional wind-tunnel model, with a chord length of $c = 0.1$ m and a span width of $b = 0.6$ m, had the DU 91-W2-250 airfoil [1,5,11] as cross section. The examined airfoil has a maximal thickness of 25 % c and had been specifically designed for the mid-span region of modern wind-turbine rotor blades. The shape of the airfoil is shown in Figure 1a; the wind-tunnel model and its instrumentation are presented in Figure 1b. The model was equipped with TSP to measure non-intrusively the surface temperature distribution on the model upper surface, and thus boundary-layer transition; moreover, TSP also allowed to examine separated flow regions at high angles-of-attack (see Sec. 3). A layer of Carbon-Nanotubes (CNT) [7,10,16-17,19] was integrated in the TSP layer composition; the CNT layer served as electrical heating to impose a temperature difference (of approx. 1-1.5 K) between model surface and flow, thus enhancing the temperature difference between the laminar and turbulent flow domains close to the model surface and enabling global and reliable transition detection via TSP. (The temperature difference imposed between flow and model surface was proven to be sufficiently low to have no appreciable influence on boundary-layer transition.) By using CNT as integrated heating, the measurement of a whole sweep of angles-of-attack (from AoA = -14° to 20° in this work) could be completed in approx. 30 minutes. TSP sensor [20], surface

quality, optical setup, acquisition and elaboration of the TSP images were the same as those discussed in [19]. In that previous work [19], TSP was also demonstrated to have no appreciable influence on the measurements of the aerodynamic coefficients, provided that the quality of the model surface with and without TSP coating was essentially the same. In the present work, the TSP surface was polished to an average roughness value of $R_a = 0.04$ μm (mean roughness depth $R_z = 0.2$ μm), i.e, to very low roughness values compatible with the thin boundary layer developing on the wind-tunnel model surface at the examined high Reynolds numbers.

As shown in Figure 1, the model was also instrumented with pressure taps to measure the surface pressure, and with a Pt100 temperature sensor to monitor the temporal evolution of the surface temperature during the experiments. The 61 pressure taps were installed in the model mid-span area and embedded in the TSP. The positions of the orifices along the airfoil contour are indicated by open circles in Figure 1a. The coefficients of airfoil lift (c_L) and pitching moment (c_m) were obtained via integration of the measured surface pressure distribution. As can be seen in Figure 1b, the pressure taps located in the region at $x/c \leq 65$ % were distributed in a staggered order, so that the measurement at any one tap was not affected by the disturbances generated by the upstream orifices, in a manner similar to that described, e.g., in [18]. The angle of these pressure tap lines about the vertical axis was approximately ±20° with respect to the freestream. The line of pressure taps located at $x/c > 65$ % was essentially parallel to the freestream: in this region, the boundary layer was expected to be turbulent at all test conditions examined in the present work, so that the measurements of these pressure taps were assumed to be not affected by the disturbances caused by the upstream orifices.

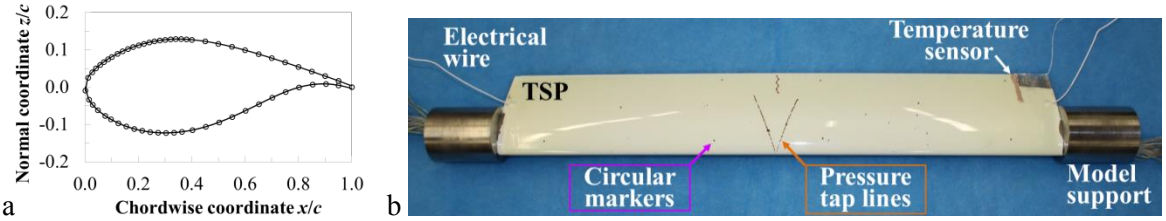

Figure 1. a: DU 91-W2-250 airfoil contour (black line) [1,5] and locations of the pressure taps (black circles); axes not equally scaled. b: top view of the instrumented model (leading edge at the bottom of the image).

The experiments were carried out in the DNW-HDG wind tunnel [9]. DNW-HDG is a closed-return wind tunnel where the air pressure can be increased up to 10 MPa. Experiments can be run at freestream velocities up to $U_\infty = 38$ m/s, thus allowing to achieve Reynolds numbers up to approx. $20 \cdot 10^6$ for a model chord length $c = 0.1$ m (as that used in the present work). A sketch of DNW-HDG is shown in Figure 2a. The test section is 1 m long and has a square cross-section with a side of 0.6 m. Experiments on two-dimensional models with $c = 0.1$ m can be conducted for a full polar of angle-of-attack, i.e., over the whole range of 360°. The flow turbulence intensity Tu in the test section is $0.2\ \% < Tu < 0.5\ \%$ for the examined Reynolds number range, where Tu was found to increase at higher Reynolds numbers [9,11-12]. Details on the DNW-HDG wind tunnel and on its instrumentation are given in [9-12,19].

A wake rake, equipped with 6 static pressure and 110 total pressure probes, was installed at a spanwise location $y/b = 0.67$ and at a distance $\Delta(x/c) = 3.4$ downstream of the model trailing edge. (y is spanwise coordinate, positive starting from the model port side and oriented towards the model starboard side.) The airfoil drag coefficient (c_D) was evaluated from the pressure distribution measured in the model wake according to the momentum theorem. Note here that the wake rake can be traversed in the spanwise direction to determine the drag coefficient at different spanwise locations and thus evaluate the impact of three-dimensional flow effects on the measured c_D of the airfoil.

An image of the experimental setup in the DNW-HDG test section is shown in Figure 2b. In this figure, the optical setup for TSP measurements (windows for camera and light-emitting diodes, i.e.,

LEDs), the wires used to supply the electrical power to the CNT and the Pt100 temperature sensor can also be seen. Note here that the electrical wires and the temperature sensor were partially exposed to the flow, but their location was at a sufficient distance from the TSP evaluation area (see Sec. 3), from the pressure taps region and from the wake rake. Therefore, the measurements of transition location and aerodynamic coefficients were not affected by disturbances induced by the wires and by the Pt100. Further details on the experimental setup and on its accuracy are provided in [19].

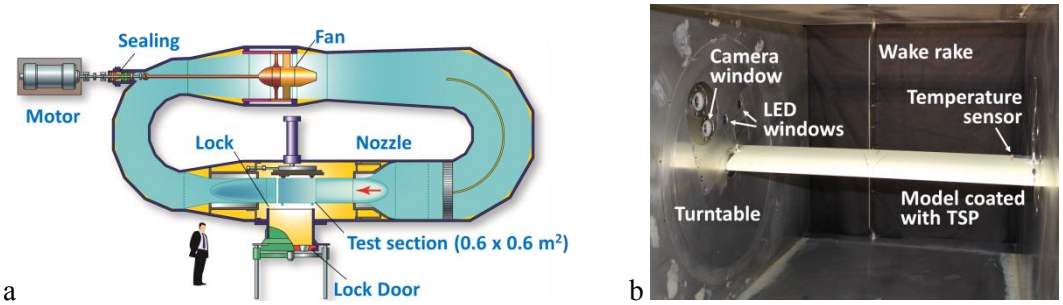

Figure 2. a: Principle sketch of the DNW-HDG wind tunnel. b: model mounted in the DNW-HDG test section, as seen from an upstream position.

3. Results and Discussion

The measurements were carried out at angles-of-attack from -14° to 20° for the following Reynolds numbers: Re = 3, 6, 9 and 12 · 10^6. The Mach number remained below M = 0.1 for all examined test conditions. As compared to previous work [19], experiments at Re = 6 and 9 · 10^6 were performed here also for an alternative combination of flow total pressure and freestream velocity, in order to examine the repeatability of the achieved results.

Example TSP results, obtained on the model upper surface at Re = 6 · 10^6, M = 0.06 (flow total pressure p_0 = 4.6 MPa) and various angles-of-attack, are presented in Figure 3. These TSP results show the wind-tunnel model as it would be seen from the top wall of the DNW-HDG test section; they were achieved after the TSP images, acquired by the camera mounted at the turntable of the test-section side wall (see Figure 2b), had been mapped onto a three-dimensional grid representing the model upper surface. This operation was performed using the DLR software package *ToPas* [21], in a manner similar to that described in [18,22]. The regions at $y/b \leq 19$ % and $y/b \geq 78$ % (i.e., those close to the test-section side walls) were masked white, since these regions were not completely visible in the TSP images and/or their spatial resolution was too low. (These limitations were due to the restricted optical access in the DNW-HDG test section – see [19].) In Figure 3, the flow is from the left; bright and dark areas correspond to regions of lower and higher heat flux, respectively, and therefore to regions of lower and higher wall shear stress. Bright and dark areas in Figure 3a-d (-12° ≤ AoA ≤ 7°) correspond to laminar and turbulent regions, respectively. The turbulent wedge observed in the mid-span area was caused by disturbances originating from the pressure taps in the leading-edge region (see [18] and [22] for a similar finding). The transition locations x_T/c and the corresponding uncertainties reported in the caption of Figure 3 were obtained as average and standard deviation of the transition locations detected at five different spanwise positions [19]. At each spanwise position, the transition location was detected as the location corresponding to the maximal gradient of the streamwise temperature distributions; this operation was performed automatically by means of a reliable algorithm described in [22]. An increase in the angle-of-attack (from left to right in Figure 3) led to a more pronounced adverse pressure gradient on the model upper surface, which induced stronger amplification of boundary-layer disturbances and thus a movement of the laminar-turbulent transition towards a more upstream location [19]. Nevertheless, the upstream shift of x_T/c in Figure 3a-c was relatively small, in spite of the considered large steps in AoA. The relative variation of the transition location as a function of the angle-of-attack remained small up to AoA = 5°; the

upstream movement of x_T/c became then more pronounced as the angle-of-attack was increased to AoA > 5°, as can be seen by a comparison of the TSP results in Figure 3c and Figure 3d. At the four highest angles-of-attack, AoA = 11°, 12°, 13° and 15° (Figure 3e-h), the flow was essentially turbulent over the whole model upper surface. At AoA = 11°, the flow was still attached over the whole model upper surface, while turbulent flow separation occurred at AoA ≥ 12°: dark and bright areas in the TSP results correspond here to attached and separated flow regions, respectively. The TSP results in Figure 3f-h also show that the separation front was not a straight line in spanwise direction. Significant spanwise variations were especially observed at stall conditions (AoA = 12°) and in the near post stall regime (13° ≤ AoA ≤ 16°), while at higher angles-of-attack (AoA > 16°) the spanwise variation of the separation front became less marked. The use of the global, non-intrusive TSP measurement technique revealed this complex flow scenario, which was very likely due to the effect of three-dimensional flow structures in the separated flow region, such as those described as "mushroom-like" structures or "owl eyes" in [23]. The dynamics of these flow structures, however, could not be captured with the adopted experimental setup, since the TSP measurements were averaged in time [19].

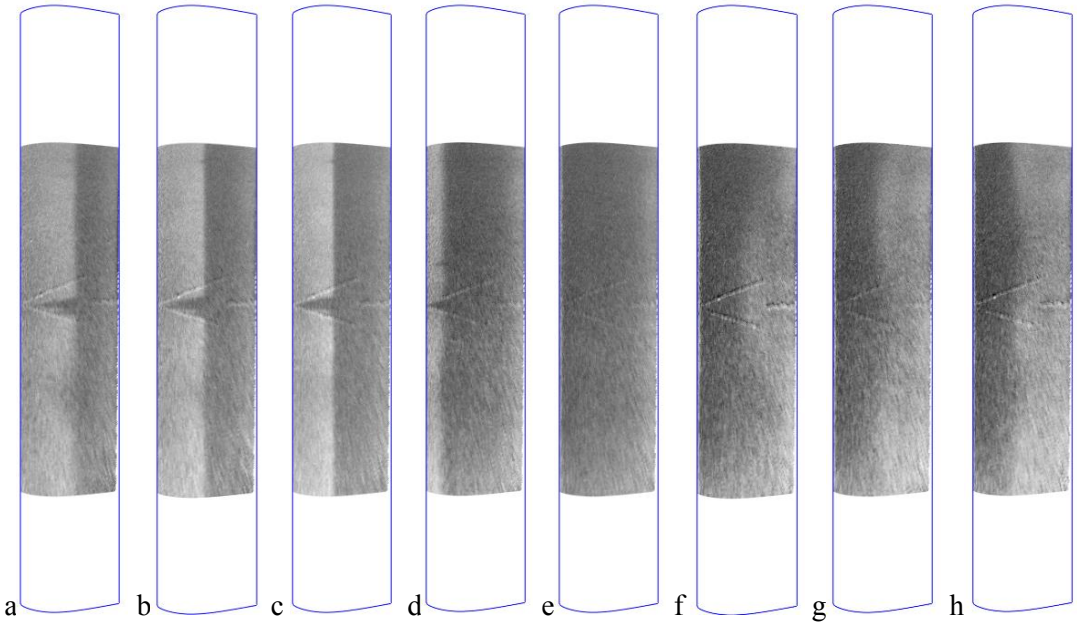

Figure 3. TSP results obtained at Re = $6 \cdot 10^6$ (M = 0.06, p_0 = 4.6 MPa) for various angles-of-attack. a: AoA = -12°, x_T/c = 54.8 ±1.0 %; b: AoA = -6°, x_T/c = 48.2 ±0.9 %; c: AoA = 0°, x_T/c = 42.6 ±0.7 %; d: AoA = 7°, x_T/c = 17.4 ±0.5 %; e: AoA = 11°; f: AoA = 12°; g: AoA = 13°; h: AoA = 15°.

The results obtained in the present study are summarized in Figure 4. The coefficients of lift, pitching moment and drag are presented as a function of the angle-of-attack in Figure 4a, Figure 4b and Figure 4c, respectively. The transition locations measured on the model upper surface by means of the TSP technique are plotted as a function of AoA in Figure 4d. In these figures, different colors show data obtained at different Reynolds numbers. Open and filled symbols correspond to the data measured at flow total pressures p_0 = 4.6 and 7 MPa, respectively. (In the legend, the corresponding data sets are indicated with (I) and (II), respectively.) The cyan rectangle in Figure 4d indicates the approximate range of AoA at which a variation in the transition location has a crucial influence on the aerodynamic performance of airfoils designed for the mid-span region of wind-turbine rotor blades [1-2,5].

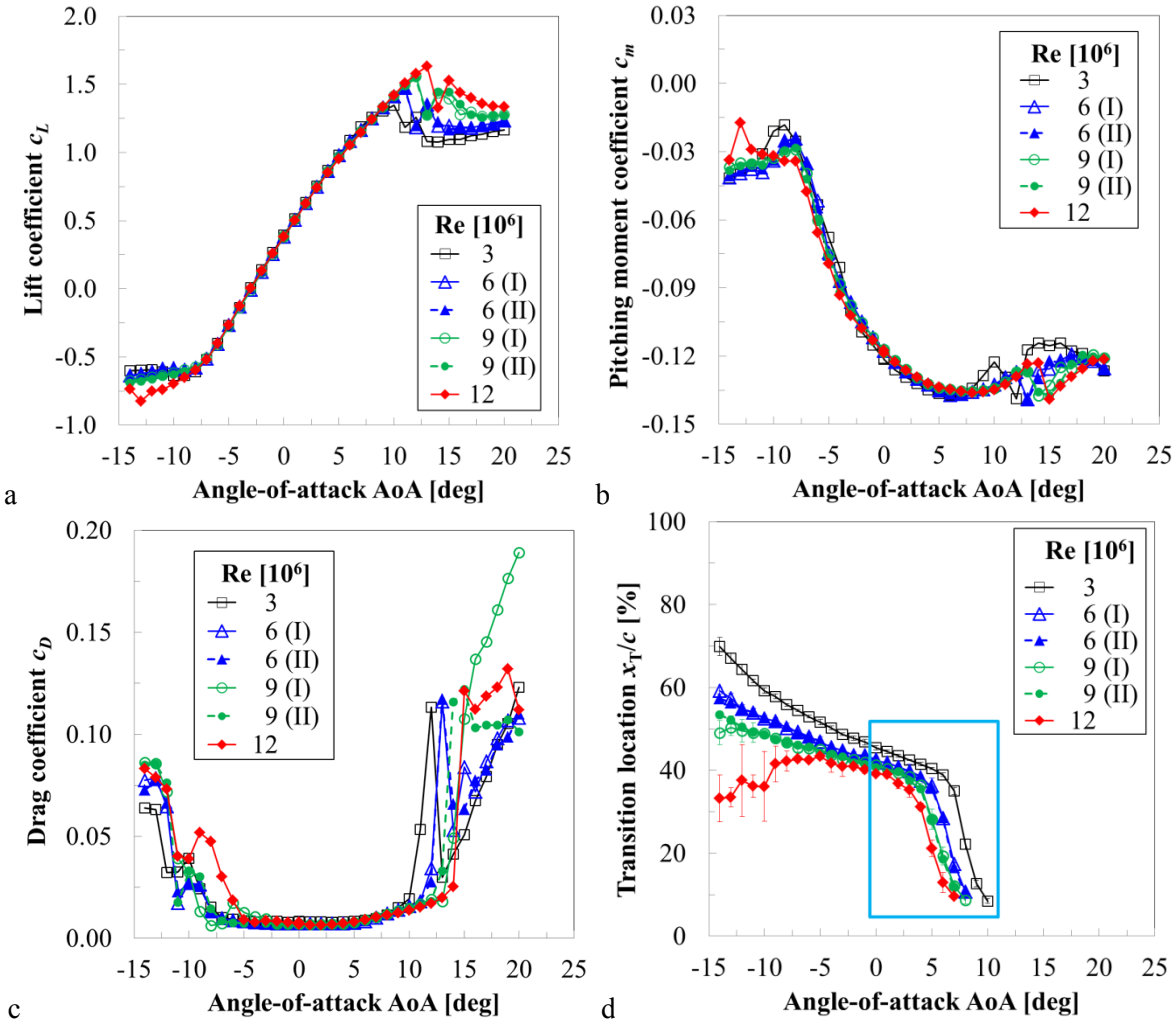

Figure 4. Aerodynamic coefficients and transition locations measured at various angles-of-attack and Reynolds numbers. a: lift coefficient; b: pitching moment coefficient; c: drag coefficient; d: transition location (upper surface).

The agreement of the lift coefficients measured at the different Reynolds numbers (Figure 4a) was excellent in the quasi-linear range of the c_L curve ($-6° \leq \text{AoA} \leq 6°$). The relative differences in the values of c_L remained below 5 % up to AoA = 10°, i.e., up to the angle-of-attack corresponding to $c_{L,\max}$ for $\text{Re} = 3 \cdot 10^6$. For each increase $\Delta\text{Re} = 3 \cdot 10^6$ in the Reynolds number, the maximal value of the lift coefficient and the value of the angle-of-attack corresponding to $c_{L,\max}$ increased consistently by approx. $\Delta c_{L,\max} = 0.1$ and by $\Delta\text{AoA} = 1°$, respectively: from $c_{L,\max} = 1.35$ (at AoA = 10°) for $\text{Re} = 3 \cdot 10^6$ to $c_{L,\max} = 1.63$ (at AoA = 13°) for $\text{Re} = 12 \cdot 10^6$. These findings are in agreement with those reported in earlier work [11]. Small differences of less than 5 % (and in most cases of less than 2 %) were observed in the pitching moment coefficients (Figure 4b) for the range of angles-of-attack $-3° \leq \text{AoA} \leq 9°$. Moreover, the evolution of c_m as a function of the angle-of-attack in the range $-8° \leq \text{AoA} \leq 10°$ was similar for all examined Reynolds numbers. In the range of angles-of-attack $-3° \leq \text{AoA} \leq 9°$, the differences in the drag coefficient (Figure 4c) were generally higher than those found for the lift and pitching moment coefficients: they were of the order of 5-10 % of the measured values of c_D. In any case, the evolution of the drag coefficient at $-4° \leq \text{AoA} \leq 10°$ was similar for all examined Reynolds numbers. At all considered angles-of-attack, transition on the model upper surface was found to occur at a more upstream location as the Reynolds number was increased (see Figure

4d). This was due to the enhanced amplification of boundary-layer disturbances at higher Reynolds numbers, which led to earlier transition. In general, the transition location was also shifted more upstream as the angle-of-attack was increased. For all examined Reynolds numbers, the relative change in transition location as a function of AoA was relatively small up to a certain angle-of-attack, corresponding to AoA = 6°, 5°, 4° and 3° for Re = 3, 6, 9 and $12 \cdot 10^6$, respectively. This was shown exemplarily for Re = $6 \cdot 10^6$ by the TSP results in Figures 3a-c. At higher angles-of-attack, the gradient $\partial(x_T/c)/\partial$AoA became more pronounced (see Figures 3c-e), until transition occurred in the leading-edge region and the boundary layer could be considered as essentially turbulent over the whole model upper surface.

Transition locations at $x_T/c < 7$ % are not reported in Figure 4d: in these cases, the evolution of boundary layer and aerodynamic coefficients was dominated by the evolution of the three-dimensional separated flow regions. As shown in Figure 3f for Re = $6 \cdot 10^6$, separation onset was found (at AoA = 12° at this Reynolds number) in the mid-span model region. However, as the angle-of-attack was increased to AoA = 13° (Figure 3g), separation was observed to occur at a more downstream location in the mid-span model area, whereas it was shifted towards a more upstream location in the neighboring regions, and in particular in the region corresponding to the wake rake location. This evolution of the separation front with increasing angle-of-attack was similar also for the two higher Reynolds numbers Re = 9 and $12 \cdot 10^6$, and provides an explanation for the different angles-of-attack corresponding to the local minima of the lift coefficient (stall conditions) and to the local maxima of the drag coefficient. In fact, as the AoA was increased up to that corresponding to stall conditions, separation occurred earlier in the pressure taps region (where c_L was evaluated) than in the wake rake region (where c_D was determined); therefore, the increase in c_D was still moderate, while c_L had significantly decreased. Similar, but opposite considerations apply for a further increase in angle-of-attack by ΔAoA = 1°: the increase in c_D was marked, while c_L had increased again. At higher angles-of-attack, the spanwise variations of the separation front became less pronounced, and the evolution of the aerodynamic coefficients was in line again. Note that the evolution of the separation front, and therefore of the aerodynamic coefficients, in the near post stall regime was slightly different at Re = $3 \cdot 10^6$, as compared to that described above for the higher Reynolds numbers. This different evolution has been discussed in [19].

The evolution of the aerodynamic coefficients at AoA < -6° was dominated by the evolution of the boundary layer on the model lower surface, and in particular by the evolution of the separated flow region on this model side for AoA < -8°. The significant increase in the drag coefficient observed at Re = $12 \cdot 10^6$ and AoA < -5° was likely due to the occurrence of one (or more) turbulent wedge(s) on the model lower surface, in a region affecting the drag measurements conducted by means of the wake rake. Unfortunately, no global information was available on the model lower surface to verify these expectations. In future investigations, TSP measurements will be carried out also on the model lower surface.

The lift and pitching moment coefficients obtained at Re = 6 and $9 \cdot 10^6$ with different combinations of flow total pressure and freestream velocity were in excellent agreement for the whole examined range of angles-of-attack, except for the data points at AoA = 15° and 16° and Re = $9 \cdot 10^6$. These differences in c_L and c_m were mainly due to small variations in the separation front and were still relatively small: within 6 % of the corresponding values of the aerodynamic coefficients. The drag coefficients were in excellent agreement at both Reynolds numbers in the range of angles-of-attack -2° ≤ AoA ≤ 11°. (At Re = $6 \cdot 10^6$, the agreement in c_D was excellent even for -10° ≤ AoA ≤ -2°.) Differences in the drag coefficient AoA ≥ 12° (i.e., at stall conditions and in the post-stall regime) were likely due to the presence, in the cases at $p_0 = 4.6$ MPa, of one or more turbulent wedges on the model lower surface, in the region where the wake rake was positioned. (The flow evolution on the model upper surface was essentially the same for both combinations of p_0 and U_∞.) The occurrence of one or more turbulent wedges was probably the reason also for the differences in c_D observed for Re = $9 \cdot 10^6$ at AoA < -2°. Unfortunately, the validity of this conjecture could not be verified in this work, since TSP measurements were not carried out on the model lower surface (see above). The

transition locations detected on the model upper surface at $Re = 6$ and $9 \cdot 10^6$ with different combinations of flow total pressure and freestream velocity were in excellent agreement for the range of angles-of-attack $-12° \leq AoA \leq 8°$. At larger angles-of-attack, the boundary layer was essentially turbulent over the whole model upper surface. The reason for the differences in the transition locations seen at $AoA < -12°$ is currently unclear. At these test conditions, the pressure distribution in the transitional region was rather flat, leading to an enhanced sensitivity of boundary-layer transition to a number of factors [22]. This topic will be the focus of future work, where experiments will be conducted at various combinations of p_0 and U_∞ for all examined Reynolds numbers. The results of these investigations may provide an explanation also for the unexpected upstream movement of the transition location observed on the model upper surface at $AoA < -5°$ and $Re = 12 \cdot 10^6$ (see Figure 4d) [19].

4. Conclusions

This contribution presents an experimental methodology to systematically analyze the aerodynamic performance of airfoils and blades designed for modern wind-turbine rotors. The methodology can be applied at flow conditions in the same range as that of real wind-turbine rotor blades and simultaneously provides aerodynamic coefficients and transition locations to verify airfoil / blade performance and to validate numerical predictions. The experimental methodology consists of conventional pressure measurements for the determination of the aerodynamic coefficients, of the TSP technique for global, non-intrusive and reliable transition detection, and of the High Pressure Wind Tunnel Göttingen to run the experiments at the same Reynolds numbers as those of real applications.

In this work, the presented methodology was demonstrated to be ready for systematic studies and productive testing. Experiments on a DU 91-W2-250 airfoil model were conducted at four different chord Reynolds numbers (from 3 to $12 \cdot 10^6$) and a wide range of angles-of-attack (from -14° to 20°), focusing on the boundary-layer evolution on the model upper surface. The data acquisition (TSP data included) for a whole sweep of angles-of-attack at a given Reynolds number was completed in approximately 30 minutes. On the model upper surface, transition was found to occur at a more upstream location as the Reynolds number was increased and, in general, also as the angle-of-attack was increased. The measurements at the two intermediate Reynolds numbers, 6 and $9 \cdot 10^6$, were performed at two different combinations of flow total pressure and aerodynamic coefficients. The aerodynamic coefficients and the transition locations, measured with the two different combinations of flow parameters, were shown to be in excellent agreement for most of the examined test conditions.

TSP was verified to be a global, non-intrusive and reliable measurement technique for transition detection at high Reynolds numbers. TSP also enabled the analysis of the evolution of the separated flow regions as a function of the angle-of-attack, thus providing an explanation for the variation of the aerodynamic coefficients observed in the near post stall regime. In fact, at these test conditions, the separation front presented significant variations in the spanwise direction, which were found to depend on angle-of-attack and Reynolds number.

Acknowledgments

The authors are grateful to: N. Falk and S. Hock (previously at DLR and TU Berlin) for the support to the TSP activities in DNW-HDG during their student projects; T. Kleindienst (DLR) and R. Lesjak (DNW) for the support during preparation of the wind-tunnel model; M. Ekert (RWTH Aachen), H. Sato and N. Tajima (Tohoku University) for the conduction and analysis of the TSP coating thickness and roughness measurements; and G. Schewe (DLR) for the helpful discussions on the boundary-layer separation behaviour of thick airfoil models at high angles-of-attack.

References

[1] van Rooij RPJOM and Timmer WA 2004 Design of Airfoils for Wind Turbine Blades *GCEP Energy Wksh.* Stanford University 26 Apr 2004.
[2] Timmer WA and Schaffarczyk AP 2004 The effect of roughness at high Reynolds numbers on

the performance of DU 97-W-300Mod *Wind Energy* **7**(4) pp 295–307.
[3] Ehrmann RS and White EB 2014 Influence of 2D Steps and Distributed Roughness on Transition on a NACA 63_3-418 *AIAA Paper* 2014-0170.
[4] Schlichting H and Gersten K 2000 Boundary–Layer Equations in Plane Flow; Plate Boundary Layer *Boundary-Layer Theory* (8^{th} ed, Berlin: Springer–Verlag) chapter 6.
[5] van Rooij RPJOM and Timmer WA 2003 Roughness Sensitivity Considerations for Thick Rotor Blade Airfoils *AIAA Paper* 2003-0350.
[6] Rebstock R, Zhai J and Schaffarczyk AP 2013 Experimental Investigation of Reynolds Number Effect on Wind Turbine Profiles in the Cryogenic Wind Tunnel Cologne DNW-KKK *J. Energy and Power Eng.* **7** pp 1957–65.
[7] Klein C, Henne U, Sachs WE, Beifuss U, Ondrus V, Bruse M, Lesjak R., Löhr M, Becher A and Zhai J 2015 Combination of Temperature-Sensitive Paint (TSP) and Carbon Nanotubes (CNT) for Transition Detection *AIAA Paper* 2015-1558.
[8] Schaffarczyk AP, Winkler H, Freudenreich K, Kaiser K and Rebstock R 2003 Reynolds Number Effects on Thick Aerodynamic Profiles for Wind Turbines *Proc. Eur. Wind Energy Conf. and Exhib.* (Brussels: EWEA) 15.
[9] Försching H, Melzer E and Schewe G 1981 Ein neuer Windkanal für gebäudeaerodynamische und -aeroelastische Untersuchungen bei Reynoldszahlen bis 10^7 *Konstr. Ingenieurbau* **35/36** pp 127–33.
[10] Klein C, Henne U, Sachs WE, Beifuss U, Ondrus V, Bruse M, Lesjak R and Löhr M 2014 Application of Carbon Nanotubes (CNT) and Temperature-Sensitive Paint (TSP) for the Detection of Boundary Layer Transition *AIAA Paper* 2014-1482.
[11] Llorente E, Gorostidi A, Jacobs M, Timmer WA, Munduate X and Pires O 2014 Wind Tunnel Tests of Wind Turbine Airfoils at High Reynolds Numbers *J. Phys.: Conf. Ser.* **524** 012012.
[12] Pires O, Munduate X, Ceyhan O, Jacobs M and Snel H 2016 Analysis of high Reynolds numbers effects on a wind turbine airfoil using 2D wind tunnel test data *J. Phys.: Conf. Ser.* **753** 022047.
[13] Quast A 2006 Detection of Transition by Infrared Image Techniques *Tech. Soar.* **30**(1/2).
[14] Gartenberg E, Johnson WG, Johnson CB, Carraway DL and Wright RE 1990 Transition Detection Studies in the Cryogenic Environment *AIAA Paper* 1990-3024.
[15] Tropea C, Yarin AL and Foss JF (eds) 2007 Transition-Detection by Temperature-Sensitive Paint *Springer Handbook of Experimental Fluid Mechanics* (Berlin: Springer-Verlag) chapter 7.4.
[16] Goodman KZ, Lipford WE and Watkins AN 2016 Boundary-Layer Detection at Cryogenic Conditions Using Temperature Sensitive Paint Coupled with a Carbon Nanotube Heating Layer *Sens.* **16**(12) 2062.
[17] Klein C, Henne U, Yorita D, Beifuss U, Ondrus V, Hensch A-K, Longo R, Hauser M, Guntermann P and Quest J 2017 Application of Carbon Nanotubes and Temperature-Sensitive Paint for the Detection of Boundary Layer Transition under Cryogenic Conditions *AIAA Paper* 2017-0336.
[18] Costantini M, Fey U, Henne U and Klein C 2015 Nonadiabatic Surface Effects on Transition Measurements Using Temperature-Sensitive Paints *AIAA J.* **53**(5) pp 1172–87.
[19] Costantini M, Fuchs C, Henne U, Klein C, Ondrus V, Bruse M, Löhr M and Jacobs M 2019 Experimental Analysis of a Wind-Turbine Rotor Blade Airfoil by means of Temperature-Sensitive Paint *AIAA Paper* 2019-0800.
[20] Ondrus V, Meier R, Klein C, Henne U, Schäferling M and Beifuss U 2015 Europium 1,3-di(thienyl)propane-1,3-diones with Outstanding Properties for Temperature Sensing *Sens. Actuator.* A: Phys. **233** pp 434–41.
[21] Klein C, Engler RH, Henne U and Sachs WE 2005 Application of pressure-sensitive paint for determination of the pressure field and calculation of the forces and moments of models in a wind tunnel *Exp. Fluids* **39** pp 475–83.

[22] Costantini M 2016 Experimental analysis of geometric, pressure gradient and surface temperature effects on boundary-layer transition in compressible high Reynolds number flow *PhD Thesis* RWTH Aachen University. https://elib.dlr.de/117965/.
[23] Schewe G 2001 Reynolds-number effects in flow around more-or-less bluff bodies *J. Wind Eng. Indust. Aerodyn.* **89** pp 1267–89.